Original Article

JCBFM

Journal of Cerebral Blood Flow & Metabolism
2021, Vol. 41(8) 2076–2089

DOI: 10.1177/0271678X21992457
journals.sagepub.com/home/jcbfm
SAGE

Detection of Alzheimer's disease-related neuroinflammation by a PET ligand selective for glial versus vascular translocator protein

Bin Ji[1], Maiko Ono[1], Tomoteru Yamasaki[2], Masayuki Fujinaga[2], Ming-Rong Zhang[2], Chie Seki[1], Ichio Aoki[3], Seiji Kito[4], Makoto Sawada[5], Tetsuya Suhara[1], Naruhiko Sahara[1] and Makoto Higuchi[1]

Abstract

A substantial and constitutive expression of translocator protein (TSPO) in cerebral blood vessels hampers the sensitive detection of neuroinflammation characterized by greatly induced TSPO expression in activated glia. Here, we conducted in vivo positron emission tomography (PET) and in vitro autoradiographic imaging of normal and TSPO-deficient mouse brains to compare the binding properties of ^{18}F-FEBMP, a relatively novel TSPO radioligand developed for human studies based on its insensitivity to a common polymorphism, with ^{11}C-PK11195, as well as other commonly used TSPO radioligands including ^{11}C-PBR28, ^{11}C-Ac5216 and ^{18}F-FEDAA1106. TSPO in cerebral vessels of normal mice was found to provide a major binding site for ^{11}C-PK11195, ^{11}C-PBR28 and ^{18}F-FEDAA1106, in contrast to no overt specific binding of ^{18}F-FEBMP and ^{11}C-Ac5216 to this vascular component. In addition, ^{18}F-FEBMP yielded PET images of microglial TSPO with a higher contrast than ^{11}C-PK11195 in a tau transgenic mouse modeling Alzheimer's disease (AD) and allied neurodegenerative tauopathies. Moreover, TSPO expression examined by immunoblotting was significantly increased in AD brains compared with healthy controls, and was well correlated with the autoradiographic binding of ^{18}F-FEBMP but not ^{11}C-PK11195. Our findings support the potential advantage of comparatively glial TSPO-selective radioligands such as ^{18}F-FEBMP for PET imaging of inflammatory glial cells.

Keywords

Alzheimer's disease (AD), glial 18-kDa translocator protein (TSPO), vascular TSPO, positron emission tomography (PET), radioligand

Received 6 October 2020; Revised 13 December 2020; Accepted 23 December 2020

Introduction

Neuroinflammation characterized by activation of glial cells is an important pathological process involved in the progression of many neurodegenerative disorders, and in particular, chronic neuroinflammation might play a critical role in the pathogenesis of certain chronic neurodegenerative diseases such as Alzheimer's

[1]Department of Functional Brain Imaging Research, National Institute of Radiological Sciences, National Institutes for Quantum and Radiological Science and Technology, Chiba, Japan
[2]Department of Radiopharmaceuticals Development, National Institute of Radiological Sciences, National Institutes for Quantum and Radiological Science and Technology, Chiba, Japan
[3]Department of Molecular Imaging and Theranostics, National Institute of Radiological Sciences, National Institutes for Quantum and Radiological Science and Technology, Chiba, Japan
[4]Research, Development and Support Center, National Institute of Radiological Sciences, National Institutes for Quantum and Radiological Science and Technology, Chiba, Japan
[5]Department of Brain Function, Research Institute of Environmental Medicine, Nagoya University, Nagoya, Aichi, Japan

Corresponding author:
Bin Ji, National Institute of Radiological Sciences, National Institutes for Quantum and Radiological Science and Technology, 4-9-1, Anagawa, Inage-ku, Chiba-shi 263-8555, Japan.
Email: ji.bin@qst.go.jp

disease (AD), and might represent a potent drug target for the treatment of neuropsychiatric disorders. Since the expression of 18-kDa translocator protein (TSPO) is greatly induced in active glial cells, until now, dozens of positron emission tomography (PET) ligands for TSPO imaging have been developed, and several in common use have been assessed quantitatively in human brain.[1] These radioligands have demonstrated a high value in visualizing neuroinflammation and its progression, as well as for monitoring treatment effects.[2–5] However, previous studies with a typical first-generation TSPO ligand, ^{11}C-PK11195, showed conflicting results regarding whether or not TSPO density is increased in patients with mild cognitive impairment (MCI) or AD,[6–10] due to low brain permeability and signal-to-noise ratio, and high plasma protein binding.[11] Although second-generation TSPO ligands have been developed to overcome this weakness, and they showed improvement in specific binding and brain permeability,[12–16] the detection of neuroinflammation with second-generation TSPO ligands is still in its infancy because almost all of them show substantial heterogeneity in their binding potentials due to a TSPO polymorphism (rs6971), which leads to three distinct binding affinity classes: high-affinity binder (HAB, Ala/Ala amino acid in position 147 of TSPO protein, major genotype) and low-affinity binder (LAB, Thr/Thr amino acid, minor genotype) express a single binding site for TSPO with either high or low affinity, respectively, whereas the mixed-affinity binder (MAB, Ala/Thr amino acid) expresses both binding sites.[17–19] Several clinical studies with second-generation TSPO radioligands failed to detect increased radioactivity retention in patients with AD, likely due to the influence of polymorphism.[12,20,21] Kreisl et al. demonstrated increased TSPO density when assessed by ^{11}C-PBR28, a well-known second-generation TSPO ligand, in the brains of patients with AD, by implementing TSPO genotype correction, as well as the positive correlation between radioligand binding and the severity of AD. TSPO polymorphism, however, still greatly interferes with its application in LAB/MAB subjects.[22] In addition to microglia, TSPO is also expressed on the endothelial layer of blood vessels, which could lead to a decrease in specificity of TSPO assessment as a biomarker of active microglia, especially in normal brain.[23–25] The development of TSPO ligand allowing the selective visualization of glial TSPO is expected to greatly improve such specificity for neuroinflammation. We originally developed a novel TSPO ligand, ^{18}F-FEBMP (2-[5-(4-fluoroethoxy-2-oxo-1,3-benzoxazol-3(2*H*)-yl)-*N*-methyl-*N*-phenylacetamide]), which is minimally influenced by TSPO polymorphism.[26] In the present study, we found that this radioligand had desirable properties regarding its selectivity for microglial TSPO binding sites and little vascular binding, thus making it superior to other tracers for detecting activation of microglia in the living mouse model and in the postmortem human brain of AD.

Materials and methods

Ethics statement

The mice studied here were maintained and handled in accordance with National Research Council's Guide for the Care and Use of Laboratory Animals and our institutional guidelines. Protocols for the present animal experiments were approved by the Animal Ethics Committees of the National Institute of Radiological Sciences, National Institutes for Quantum and Radiological Science and Technology. Animal welfare was assessed daily by staff of the animal facility. Experiments were performed and reported in accordance with the ARRIVE (Animal Research: Reporting in Vivo Experiments) guidelines. All experiments were performed in a blinded manner.

Reagents and antibodies

The following reagents were of analytical grade and were commercially purchased: PK11195 and bovine serum albumin (BSA) from Sigma-Aldrich (St. Louis, MO). All other chemicals were also of analytical grade and commercially available.

The following commercial antibodies were employed in this study: rabbit polyclonal antibodies against ionized calcium binding adapter molecule-1 (Iba-1) (Wako Pure Chemicals, Osaka, Japan), rat monoclonal antibody against mouse Mac-1 (M1/70) (BMA Biomedicals, Rheinstrasse, Switzerland), rat monoclonal antibody against GFAP 2.2B10; Zymed/Invitrogen, Carlsbad, CA), mouse monoclonal antibody against human HLA-DP, DQ, DR (clone CR3/43; Dako, Carpinteria, CA), and rabbit polyclonal antibodies against TSPO (ab92291, Abcam, Cambridge, UK; indicated as commercially available (C.A.) anti-TSPO antibody for immunohistochemical and immunoblot analyses). Additionally, we also used two originally developed antibodies, NP155[27] and NP157,[28] for biochemical analyses of rodent and human TSPO, respectively.

Animal models

Tg mice heterozygous for human T34 (4-repeat tau isoform with 1 N-terminal insert) with FTLD-17 P301S mutation driven by mouse prion protein promoter (PrP), also referred to as PS19 mice,[29] were bred and kept on a C57BL/6 background. Global TSPO-KO

mice were generated through the targeted deletion of exons 2 and 3. The targeting construct was electroporated into C57BL/6 embryonic stem cells for homologous recombination. Correctly targeted cells were injected into C57BL/6 blastocysts generating chimeric mice. Female TSPOfl/fl mice were crossed with male CaMKIIa-Cre mice (RIKEN C57BL/6-TgN(a-CaMKII-nlCre)/10) expressing Cre in germ cells, generating heterozygous global TSPO-KO mice. Mice were bred to C57BL/6J mice (CLEAR, Japan) to remove the Cre transgene.[30] The information of gender and age of the animals used was indicated in the corresponding figure legends. All mice studied here were maintained and handled in accordance with the National Research Council's Guide for the Care and Use of Laboratory Animals and our institutional guidelines. Protocols for the present animal experiments were approved by the Animal Ethics Committees of the National Institute of Radiological Sciences.

In-vitro autoradiography

Postmortem human brains for *in-vitro* autoradiographic analysis were obtained from the Center for Neurodegenerative Disease Research at the University of Pennsylvania Perelman School of Medicine. The brains were cut into 20-μm-thick sections and stored at −80°C until use. For *in-vitro* autoradiographic experiments, the brain sections were preincubated with Tris-HCl buffer for 30 min, followed by incubation with radiolabelled ligands (^{18}F-FEBMP (0.5 nM) or ^{11}C-PK11195 (1 nM)) in 50 mM Tris-HCl buffer containing 5% ethanol at room temperature for 1 h. To determine the specific binding of these radioligands for TSPO, unlabelled PK11195 (10 μM) was added to the incubation solution in advance. After that, the sections were rinsed with ice-cold wash buffer (50 mM Tris-HCl buffer containing 5% ethanol) twice for 2 min each time and finally dipped into distilled water for 10 sec. The sections were dried with warm blowing air and then attached to an imaging plate (BAS-MS2025; GE Healthcare, Piscateway, NJ) for optimized contact periods. Radioactivity was detected by scanning the imaging plate using the BAS-5000 system (FUJIFILM, Tokyo, Japan). ROIs were carefully placed on grey matter of the frontal cortex, and radioactivity was expressed as photo-stimulated luminescence (PSL) per unit area (PSL/mm^2).

Immunohistochemical and histochemical analyses

Mice were deeply anesthetized with sodium pentobarbital and transcardially perfused with phosphate-buffered saline. Brain tissues were removed, were fixed with 4% paraformaldehyde in phosphate buffer (PB) overnight, and then cryoprotected with 30% sucrose in PB. Ten-μm-thick frozen sections were generated in the cryostat (HM560; Carl Zeiss, Jena, Germany) and immunostained using fluorophore-conjugated secondary antibodies (Molecular Probes/Invitrogen, Eugene, OR). All stained samples were examined with an all-in-one fluorescence microscope (BZ-9000; Keyence, Osaka, Japan), which was capable of tiling photomicrographs and merging them into a high-resolution image with a large field of view.

Western blot

Samples (5 μg protein) of human tissue were applied to a 20% sodium dodecyl sulfate polyacrylamide gel. Following electrophoresis and transfer of proteins to a polyvinylidene fluoride membrane (Immobilon P; Millipore, Tokyo, Japan), the membrane was immersed in Tris-buffered saline (150 mM NaCl, 10 mM Tris-HCl, pH 8.0) containing 0.05% (v/v) Tween 20 and 3% (w/v) bovine serum albumin, and then reacted with commercial or original antibodies (all antibodies were diluted to 1:1000) in TBS containing 0.05% (v/v) Tween 20 and 0.1% (w/v) BSA overnight. Primary antibodies were detected by HRP-conjugated anti-IgG antibodies (Amersham Pharmacia Biotech/GE Healthcare, Piscateway, NJ) and enhanced chemiluminescence method (Amersham Pharmacia Biotech/GE Healthcare).

Magnetic resonance imaging (MRI) of mouse brains

PS19 mice were anesthetized with 1.5% (v/v) isoflurane and held in place by ear bars and hard facemasks during the MRI scans. T2-weighted 2 D multi-slice spin-echo (rapid acquisition with relaxation enhancement; RARE) was applied to the mouse heads by the 7.0-Tesla MRI system (Bruker BioSpin, AVANCE-III, Karlsruhe, Germany) with a volume coil for transmission (Bruker BioSpin) and a quadrature surface coil for reception (Rapid Biomedical, Rimpar, Germany) with the following parameters: repetition time (TR) = 4200 ms, effective echo time (TE) = 36 ms, field of view (FOV) = 25.6 × 14.5 mm^2, slice thickness = 0.5 mm, number of slices = 28 (non-gap), matrix = 256 × 256, number of acquisitions (NA) = 8, nominal in-plane resolution = 100 × 57 μm^2, RARE factor = 8.

Radiosynthesis of radioligands and small animal PET imaging

Radiosynthesis of ^{11}C-PK11195 and ^{18}F-FEBMP (2-[5-(4-fluoroethoxy-2-oxo-1,3-benzoxazol-3(2*H*)-yl)-*N*-methyl-*N*-phenylacetamide]) was performed as described in previous studies,[26] and the radiochemical purity of these ligands was >95%. The specific

radioactivity of ^{11}C-PK11195 and ^{18}F-FEBMP was 35-84 GBq/μmol at the end of synthesis.

PET scans were performed by microPET Focus 220 animal scanner (Siemens Medical Solutions USA, Knoxville, TN) as described elsewhere.[27] Mice were anesthetized with 1.5% (v/v) isoflurane, and a 30-G needle connected to a 1-ml polypropylene syringe via a length of polyethylene tubing was inserted into the tail vein. Emission scans were acquired for 60 min in 3 D list mode with an energy window of 350-750 keV, immediately after ^{11}C-PK11195 (29∼38 MBq) or ^{18}F-FEBMP (13-15 MBq) was intravenously injected. Images were reconstructed by either maximum a posteriori method or filtered back-projection using a 0.5-mm Hanning filter. Volumes of interest (VOIs) were placed on the hippocampus and striatum (ST) of wild type, TSPO-KO and PS19 mice in a blinded manner, using PMOD® image analysis software (PMOD Technologies Ltd, Zurich, Switzerland) with reference to individual MRI T2-weight images for PS19 Tg mice or an MRI brain template [14] for wild-type (WT) and TSPO-KO mice. Tracer uptake in each VOI was estimated as the percentage of injected dose per tissue volume (%ID/ml). Binding potential (BPnd) was calculated by a simplified reference tissue model with ST as reference tissue, as there is no observable tau lesion and related gliosis in PS19 mice, making ST available as reference tissue in quantitative analysis for TSPO imaging of PS19 mice.[14]

Statistical analysis

All statistical examinations in the present study were performed with SPSS software. The difference between groups was considered significant at $p < 0.05$.

Results

Detecting basal TSPO expression in normal brain

First, PET scans with ^{18}F-FEBMP and ^{11}C-PK11195 in normal mouse and an originally developed TSPO knockout (TSPO-KO) mouse were performed. There was evidence of brain retention of ^{11}C-PK11195 in normal mouse brain compared with TSPO-KO mouse, whereas no similar increase in retention of ^{18}F-FEBMP was detected. In contrast, there was increased brain uptake at later phase in TSPO-KO mouse compared with normal mouse, likely due to brain uptake of radioactive metabolites massively generated under the lack of peripheral binding sites for ^{18}F-FEBMP (Figure 1). Two widely used second-generation TSPO radioligands, ^{18}F-FEDAA1106 and ^{11}C-PBR28, showed similar characteristics to ^{11}C-PK11195, while ^{11}C-Ac5216 showed results similar to ^{18}F-FEBMP (Supplemental Materials; SFigure 1). *In-vitro* autoradiogram also showed a similar result to *in-vivo* imaging. There was no overt specific binding of ^{18}F-FEBMP and ^{11}C-PK11195 in whole brain of TSPO-KO mouse (ratio of total binding to non-specific binding was approximately 1, indicating that a very small portion of total binding was specific binding). Except for cerebral ventricles and cerebellum enriched with TSPO expression, ^{18}F-FEBMP showed faint specific binding in normal mouse brain, while there was overt specific binding of ^{11}C-PK11195 (ratio of total binding to non-specific binding was approximately 4, indicating that approximately 75% of total binding was specific binding) in whole brain with especially higher radiolabeling in cerebral ventricles and cerebellum (Figure 2(a) and (b)). All of these results indicated that ^{11}C-PK11195 more sensitively detected TSPO expression in normal mouse compared with ^{18}F-FEBMP. Double-channel immunohistochemistry clearly demonstrated a major origin of TSPO from blood vessels and a minor origin from resident astrocytes in normal mouse brain. Microglial TSPO was marginally detectable under normal conditions (Figure 2(c) to (j)).

Neuroinflammation in AD model and postmortem AD brains

We performed dual PET scans with ^{18}F-FEBMP and ^{11}C-PK11195 in a transgenic mouse line (PS19) with age-dependent brain atrophy and gliosis to examine the sensitivity of ^{18}F-FEBMP for detecting TSPO induction in activated glia in the living brain. The increase in radioligand binding in the hippocampus with less atrophy was more easily judged by visual images of ^{18}F-FEBMP than ^{11}C-PK11195, although increased radioactivity was visually realized by PET images of both radioligands in the mouse with severe pathology. Quantitative analysis for binding potential (BPnd) including three non-Tg and three Tg mice with a simplified reference tissue model using the striatum as reference tissue showed statistically significant difference in BPnd of ^{18}F-FEBMP, but not ^{11}C-PK11195, between the non-Tg and Tg groups, indicating superiority of ^{18}F-FEBMP in stability and sensitivity for *in-vivo* measurement of neuroinflammation compared with ^{11}C-PK11195 (Figure 3). Double-channel immunohistochemical analysis clearly demonstrated dominant TSPO expression in activated microglia and astrocytes in the lesioned hippocampus of Tg mouse (Figure 4).

In-vitro autoradiographic analysis of five postmortem brains of healthy control (HC) and AD, respectively, showed significant increase in binding of ^{18}F-FEBMP in gray matter of the temporal cortex of AD compared with HC, while there was no significant difference in binding of ^{11}C-PK11195

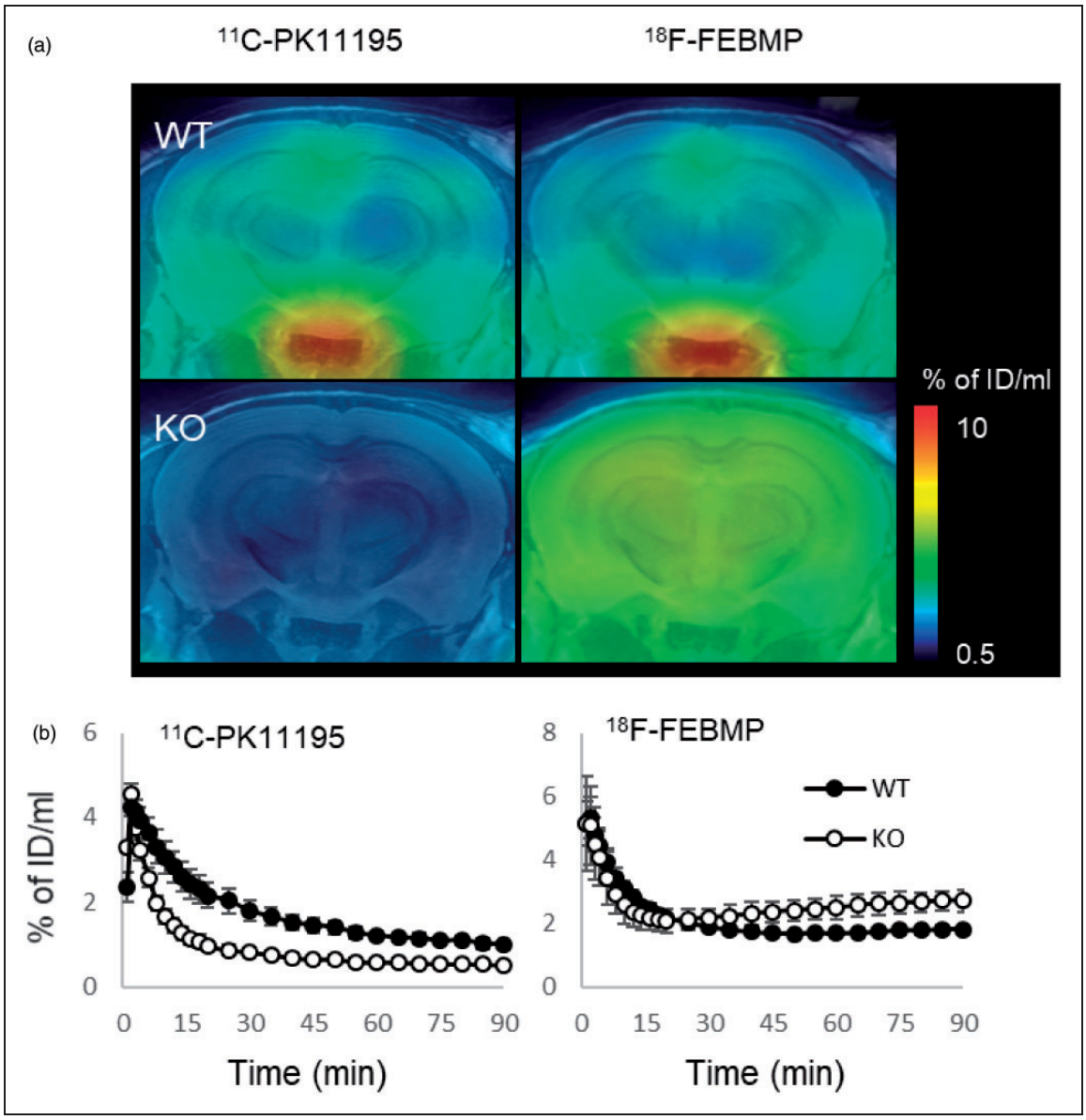

Figure 1. *In-vivo* PET images of brains of WT and TSPO-KO mice following intravenous injection of TSPO radioligands. A: The representative ^{11}C-PK11195 and ^{18}F-FEBMP PET images of coronal mouse brain sections (2.4 mm posterior to the bregma) containing the neocortex and hippocampus in WT (male, 2-month old) and TSPO-KO (male, 2-month old) mice. PET images generated from averaged dynamic data (30–60 min) are overlapped with the MRI template of mouse coronal brain sections. B: Brain uptake was expressed as percentage of injected dose per ml brain volume in hippocampi from WT and TSPO-KO mice (each group included four 2-month-old male mice) over the scan time. The same individuals were used for ^{11}C-PK11195 and ^{18}F-FEBMP scans. Error bars represent standard deviation (SD). WT: wild-type, KO: TSPO-KO.

(Figure 5(a) and (b)). Double-channel images showed numerous TSPO-positive ramified microglia in aged HC brain, while vascular TSPO was still in the majority. TSPO-enriched microglia with hypertrophic morphology became evident, although morphologically activated astrocytes expressed faint TSPO in the frontal cortex of AD brain (Figure 5(c) and (l)). Immunoblot analysis with two anti-TSPO antibodies showed that the protein expression of TSPO was significantly induced in the AD brain sample as compared with HC. Interestingly, *in-vitro* binding of ^{18}F-FEBMP showed positive correlation with the TSPO protein expression level, while no correlation was detected between the binding of ^{11}C-PK11195 and TSPO expression examined by the two anti-TSPO antibodies (Figure 6).

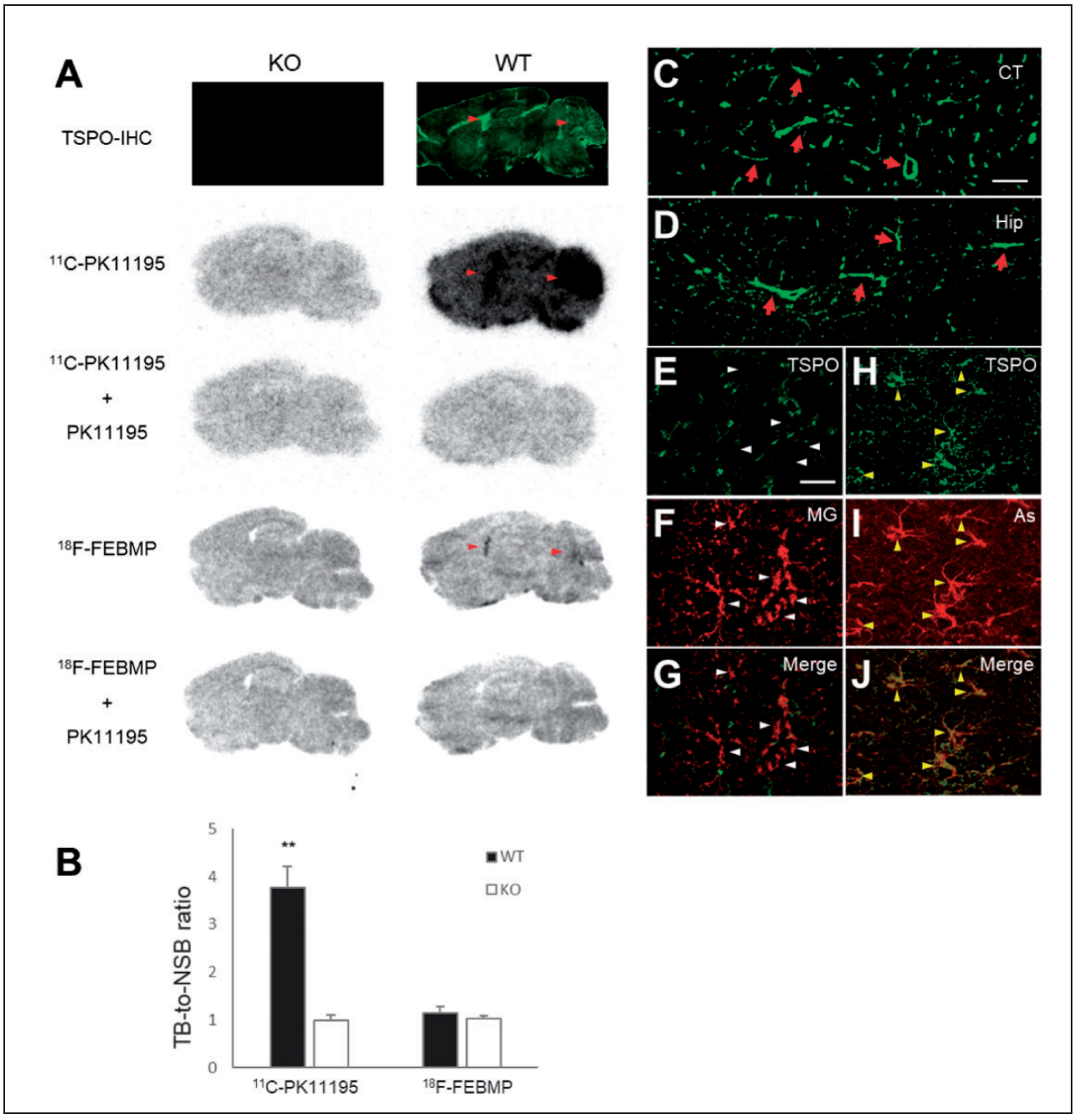

Figure 2. Origin of TSPO expression and binding of radioligands in normal mouse brain. A: Immunohistochemistry with commercially available (C.A.) anti-TSPO antibody and representative *in-vitro* autoradiographic images of ^{11}C-PK11195 and ^{18}F-FEBMP in sagittal mouse brain sections from TSPO-KO (left) and WT (right) mice. Red arrowheads indicate lateral ventricles and cerebellums. B: Quantitative analysis for *in-vitro* binding. Data were from panel A. Total binding (TB) and non-specific binding (NSB) were calculated in the absence and presence of non-radiolabeled PK11195, respectively. Brain sections from six TSPO-KO and six WT mice were used for autoradiography with ^{11}C-PK11195, and brain sections of three mice among the six TSPO-KO and WT mice, respectively, were used for autoradiography with ^{18}F-FEBMP. There were significant main effects of genotype and tracer on *in-vitro* binding, [$F_{(1,\ 14)} = 83.92$ and 105.7, respectively, $p < 0.0001$ by two-way ANOVA]. TB-to-NSB ratio of ^{11}C-PK11195 in WT brain was significantly higher than in other three groups (**, $p < 0.01$ by *post hoc* Bonferroni's test), while that of ^{18}F-FEBMP in WT brain was similar to that in KO mouse groups ($p > 0.99$ by *post hoc* Bonferroni's test). Error bars represent SD. C, D: Immunohistochemical analysis for TSPO origin. Most immunoreactivity of anti-TSPO antibody was from blood vessels (arrows in C and D) as shown in representative images of cortical and hippocampal regions. E-J: Double-channel photomicrographs of immunostaining of TSPO (E, H, and green in merged images G, J) and either microglia (MG; F and red in merged image G) or astrocytes (As; I and red in merged image J) demonstrated that resident astrocytes, but not microglia, express detectable TSPO in normal mouse brain. Scale bars: 50 μm (C, D); 20 μm (E-J).

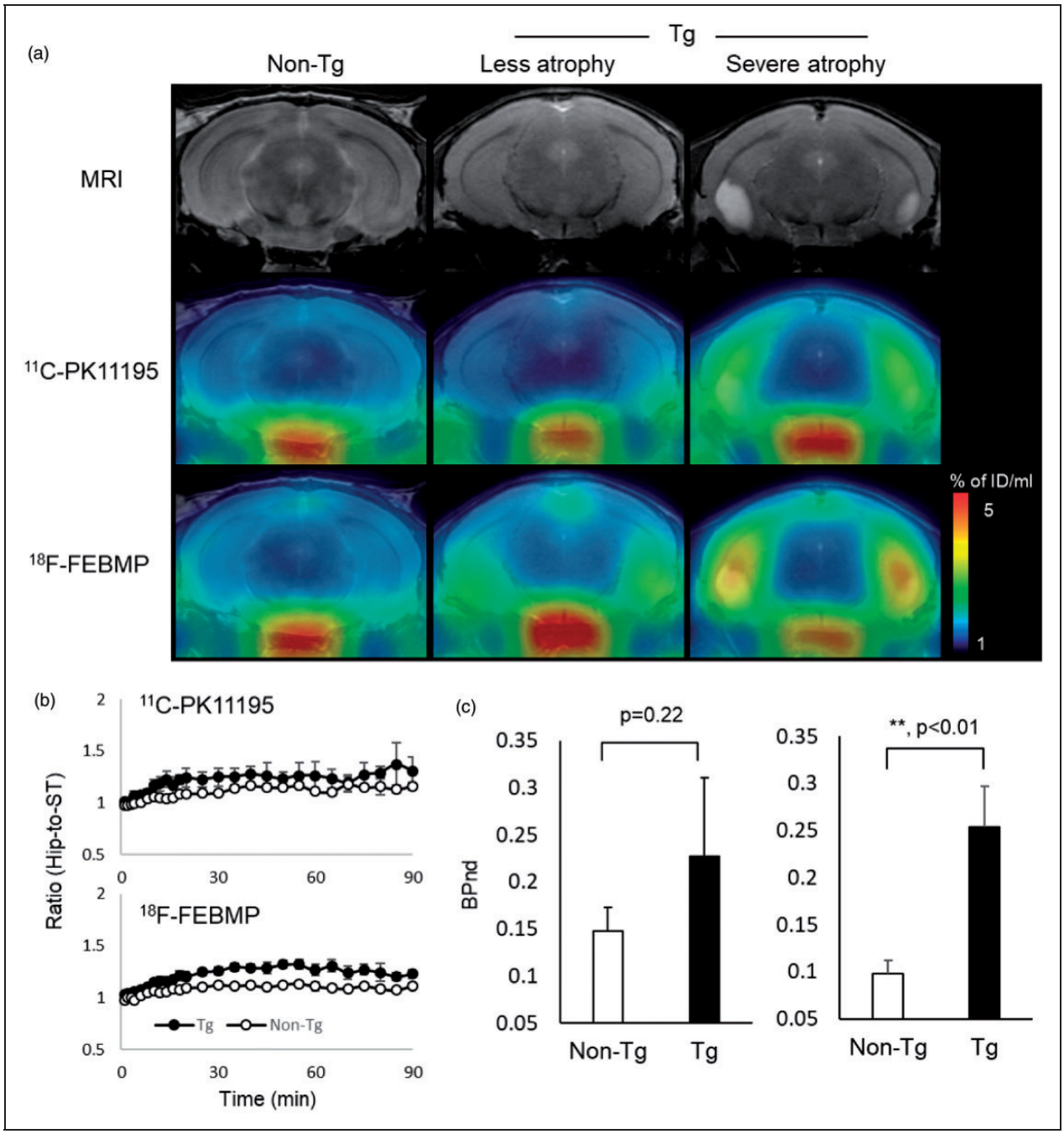

Figure 3. Tau lesion-associated microglial TSPO was more sensitively captured by *in-vivo* PET imaging with ^{18}F-FEBMP than ^{11}C-PK11195. A: T2 MRI images (upper row) and PET images with ^{18}F-FEBMP (middle row) and ^{11}C-PK11195 (lower row) of coronal mouse brain sections (2.8 mm posterior to the bregma) containing the neocortex and hippocampus in a male non-Tg (left column), and male PS19 Tg individuals with less (middle column) and severe (right column) brain atrophy at 9 months. The PET images generated from averaged dynamic data (30–60 min) are overlapped with the respective MRI brain templates (adult C57BL/6J) of coronal brain sections of individual mice. The images of middle (less atrophy) and right (severe atrophy) columns were from the same individuals, respectively. B: Time course of hippocampus (Hip)-to-striatum (ST) ratios of radioactivity of ^{11}C-PK11195 (upper) and ^{18}F-FEBMP (lower) C: Binding potential (BPnd) calculated by simplified reference tissue model with ST as reference tissue showing *in-vivo* binding of ^{18}F-FEBMP (right), but not ^{11}C-PK11195 (left), was significantly increased in Tg compared with non-Tg mice ($n = 3$ and $n = 4$ for 8-month-old male PS19 and age-matched non-Tg mice, respectively; $t = -3.868$, *, $p < 0.05$ by independent t-test for ^{18}F-FEBMP). The same individuals were used for in vivo imaging of ^{11}C-PK11195 and ^{18}F-FEBMP. Error bars represent SD.

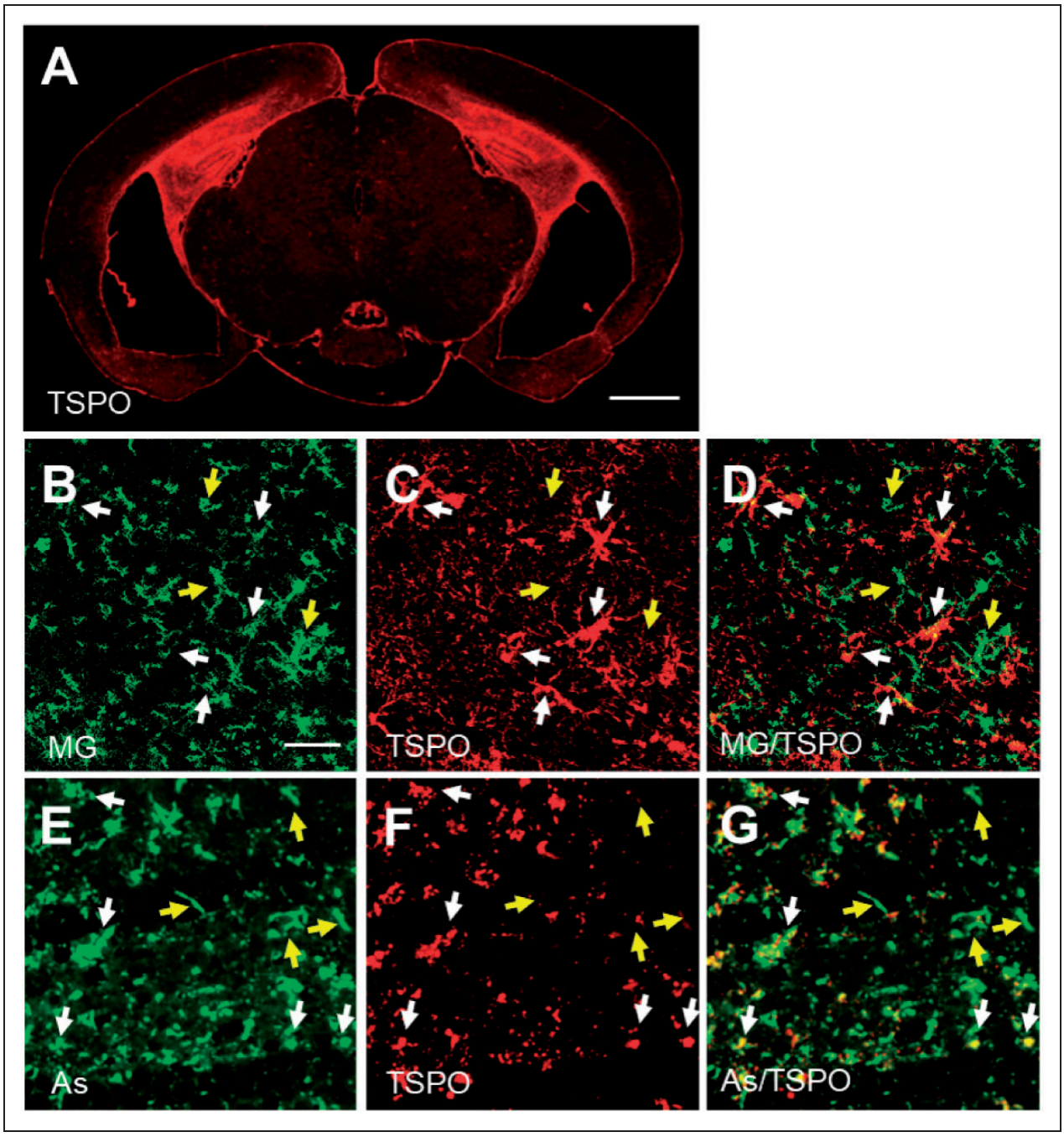

Figure 4. Immunohistochemical analysis for TSPO origin in PS19 mouse. The immunoreactivity of anti-TSPO antibody was greatly increased in hippocampus of Tg mouse individual with overt brain atrophy (A), and double-channel photomicrographs of immunostaining of either microglia (MG; B and green in merged image D) or astrocytes (As; E and green in merged image G) and TSPO (C, F and red in merged images D, G) demonstrated that the majority of TSPO was activated microglia (white arrows in B-D) and astrocytes (white arrows in E-G), although there was still a subset of microglia and astrocytes lacking overt TSPO expression (yellow arrows in B-G) in lesioned hippocampus of Tg mouse. A part of TSPO-positive astrocytes seemed to be blood vessel-associated subtype morphologically. Scale bars: 1 mm (A); 20 μm (B-G).

Discussion

Non-invasive measurement with TSPO imaging in combination with other core pathologies such as senile plaques and neurofibrillary tangles consisting of amyloid-β (Aβ) and tau protein deposits, respectively, in patients with MCI/AD, would be greatly informative and helpful for predicting the prognosis and clarifying the interactive relationships between

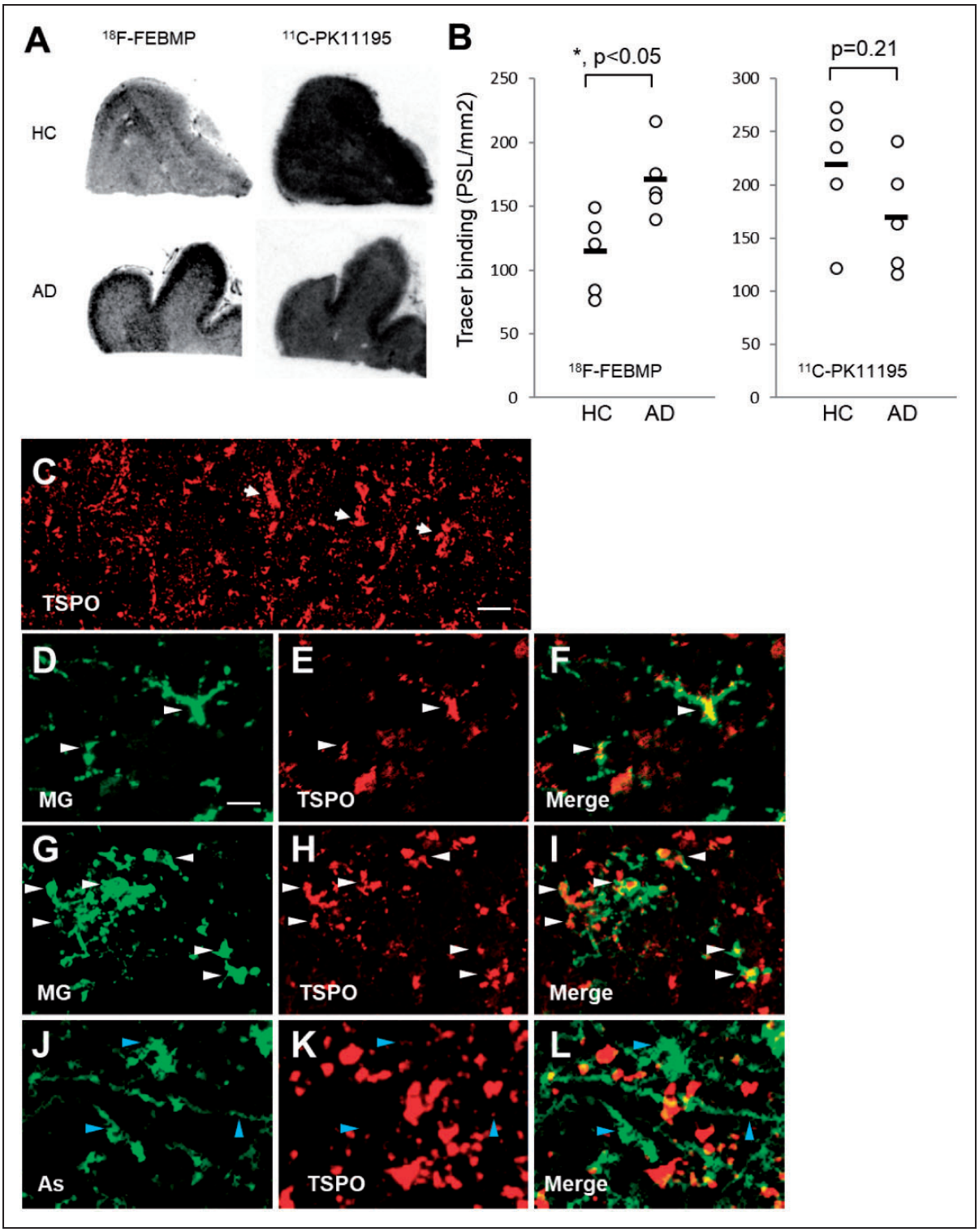

Figure 5. *In-vitro* autoradiographic and immunohistochemical analysis in postmortem brains from healthy control (HC) and patients with AD. A: Representative *in-vitro* autoradiographic images of ^{11}C-PK11195 (right) and ^{18}F-FEBMP (left). B: Quantitative analysis for specific binding of radioligands. *In-vitro* binding of ^{18}F-FEBMP, but not ^{11}C-PK11195, was significantly increased in gray matter of frontal cortex from AD compared with a similar region of HC ($n = 5$ in each group, $t = -2.983$, *, $p < 0.05$, by independent t-test for ^{18}F-FEBMP). Data were from autoradiographic analysis as shown in panel A. Short horizontal lines indicate average values of groups. Error bars represent SD. C-L: Immunohistochemical analysis in frontal cortex of HC (C-F) and AD (G-L) brains. Arrows in low-power image (C) indicate TSPO expressed on morphologically typical blood vessels. Double-channel photomicrographs of immunostaining of TSPO (E, H, K and red in merged images F, I, L) and either microglia (MG; D, G and green in merged image F, I) or astrocytes (As; J and green in merged image L) demonstrated that TSPO-positive microglia were observable in both HC and AD brains, while astrocytes expressed TSPO poorly even in AD brain. White (D-I) and blue (J-L) arrowheads indicate TSPO-positive microglia and TSPO-negative astrocytes, respectively. Scale bars: 50 μm (C); 20 μm (D-L).

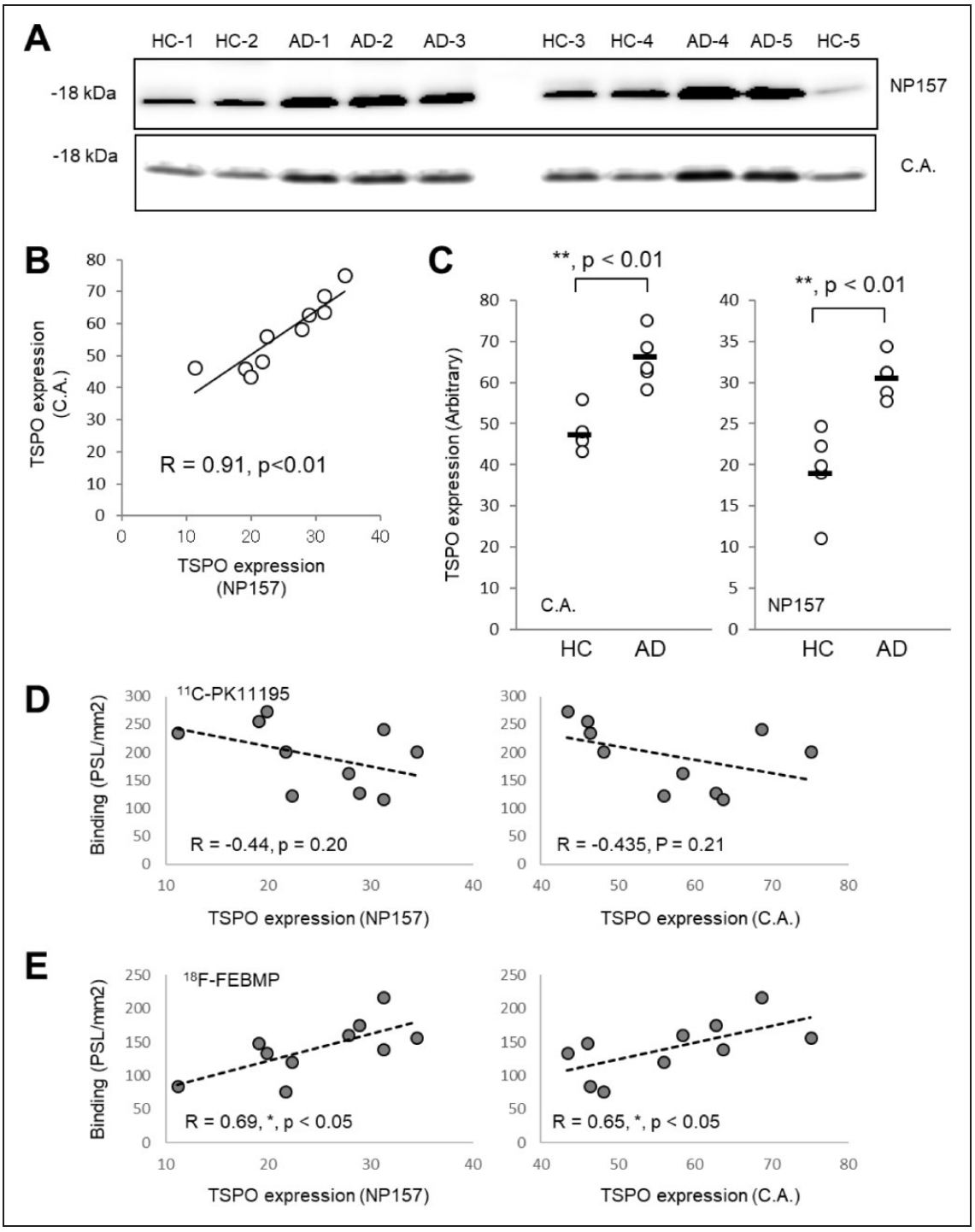

Figure 6. Correlations between TSPO expression and *in-vivo* binding of radioligands in human brains. A-C: Western blot analysis of TSPO expression in gray matter of frontal cortex (same individuals as determined in autoradiogram) with an original antibody, NP157, and commercially available (C.A.) antibody (A). Quantitative analysis showed excellent correlation between TSPO expression determined by these two antibodies (B), and significant increase in TSPO expression detected by either C.A. or NP157 in AD brain compared with HC ($n = 5$ in each group, $t = -4.971$, $^{**}p < 0.01$, by independent t-test, for C.A., $t = -4.404$, $^{**}p < 0.01$, by independent t-test, for NP157). D, E: The correlation between *in-vitro* binding of ^{11}C-PK11195 and TSPO expression detected by immunoblot with either C.A. or NP157 was not significant (D), and similar analysis demonstrated significant positive correlations between *in-vitro* binding of ^{18}F-FEBMP and TSPO expression detected by immunoblot with either C.A. or NP157 (E). Data were from immunoblotting and autoradiographic analyses shown in panel A and Figure 4, respectively. Correlation between two parameters was examined by parametric test with Pearson product-moment correlation coefficient (R).

pathological changes as well as for developing specific treatments.[14,27,28,31,32] However, *in-vivo* TSPO imaging with ^{11}C-PK11195 showed conflicting results regarding whether or not TSPO is induced in MCI or AD.[6–10] We also failed to detect the increase in TSPO amount determined by autoradiography with ^{11}C-PK11195 in AD brains. These results raise a concern regarding the sensitivity of PET with ^{11}C-PK11195 for quantifying TSPO density in human subjects with chronic and mild-level neuroinflammation.

Although TSPO is considered an imaging biomarker for the activation of microglia in response to neuronal lesions, basal expression with origins in blood vessels and resident astrocytes is also detectable in normal human and rodent brains, as shown in the present study (Figure 2) and a previous publication.[23] Vascular TSPO is considered to greatly contribute to the binding sites for TSPO ligands in normal brain, and kinetic modeling without accounting for vascular components has led to overestimation of microglial binding.[24,25] The fact that there is little binding of FEBMP to vascular TSPO expression is considered to greatly contribute to the sensitive detection of neuroinflammation with glial TSPO induction.

Considering the possible decrease in lumen size and the loss of vascular TSPO caused by vascular fibrosis in AD brain,[25] examination for the induction of TSPO expression in AD brain by biochemical methods has become an urgent matter. To the best of our knowledge, until now there has been no such clear demonstration. In the present study, immunoblotting analysis with two specific anti-TSPO antibodies and immunohistochemistry clearly indicated an increase of AD pathology-associated TSPO expression. This result supports the current concept of TSPO as a useful biomarker of neuroinflammation, and indicates the advantage of using ^{18}F-FEBMP, binding of which is linearly correlated with TSPO expression (Figure 6), for neuroinflammation detection. It is unclear why FEBMP shows different binding characteristics from PK11195 in mouse and human brains. Combined with the fact that PK11195 showed significant differences in dissociation constant between brain regions of Landrace pigs, suggesting the heterogeneity of PK11195 binding sites,[33] we propose the following hypothetical scenario: there are two binding sites for PK11195 provided by only TSPO molecules and an unconfirmed component X, respectively, while only TSPO molecules provide a binding site for FEBMP. Thus the amount of TSPO molecules is linearly proportional to FEBMP binding, but does not solely govern PK11195 binding. The candidate of component X includes TSPO polymers and a complex formed by voltage-dependent anion channel (VDAC) and TSPO.[34,35] UV-irradiation-induced polymerization of recombinant TSPO increased the binding of PK11195, while it decreased the binding of cholesterol in a test tube.[35] VDAC is a constitutive protein of mitochondria and contributes to the binding site for PK11195 in combination with adenine nucleotide carrier and TSPO.[36,37] AD-related pathological molecules may change the VDAC location and amount[38–40] and therefore change VDAC-associated binding sites. This might explain why PK11195 binding correlates poorly with TSPO expression in AD brain. Heterogeneous distribution of component X in vascular and glial departments may be responsible for the different binding characteristics between PK11195 and FEBMP shown in the present study. To more clearly demonstrate the preferential binding of TSPO ligands, we are generating microglia-selective TSPO-KO mice, and we have an experimental plan to test the *in-vivo* and *in-vitro* bindings of FEBMP and other TSPO ligands under physiological and pathological conditions with this newly-developed mouse model. Here, we propose that there are at least two types of binding sites, vascular vessel-like and glia-like, for TSPO ligands. According to the ability to detect basal TSPO in normal mouse brain, ^{11}C-PK11195, ^{11}C-PBR28 and ^{18}F-FEDAA1106 were classified as high detectability of vascular TSPO ligands, and ^{18}F-FEBMP and ^{11}C-Ac5216 were classified with low detectability of vascular TSPO ligands (Figure 7). Although ^{11}C-Ac5216 showed high selectivity for glial TSPO, similar to ^{18}F-FEBMP, we failed to detect any significant increase in ^{11}C-Ac5216 binding to the same AD samples used here without genetic examination (data not shown), likely due to the major influence of TSPO polymorphism ($R_{Ki(L/H)}$ of Ac5216 was the highest after PBR28).[17,18] ^{18}F-FEBMP has none of the above-mentioned disadvantages of ^{11}C-Ac5216, and is therefore considered a suitable candidate for detecting neuroinflammation in preclinical and possibly upcoming clinical studies. Given its possible metabolic instability, ^{18}F-FEBMP may not be a perfect ligand for clinical use. The present data showed an increase in brain uptake at the later phase in TSPO-KO mice, but not in normal mice (Figure 1), suggesting the generation of brain-permeable radioactive metabolites likely due to a lack of peripheral binding sites. Although massive metabolites are inconvenient for neuroinflammation imaging, this obstacle may be minimized under the common condition of abundant peripheral binding sites for TSPO tracers. Our previous study also showed that intact ^{18}F-FEBMP in the brains of a rat model with focal ischemia remained at $83.1 \pm 7.3\%$ and $76.4 \pm 2.1\%$ at 30 and 60 min post-injection, respectively.[26] FEBMP seems not to exclusively bind to glial TSPO, because *in-vitro* autoradiography with ^{18}F-FEBMP shows limited specific binding in cerebral ventricles and cerebellum of WT mouse (Figure 2), where there is no greater abundance of glia than in other

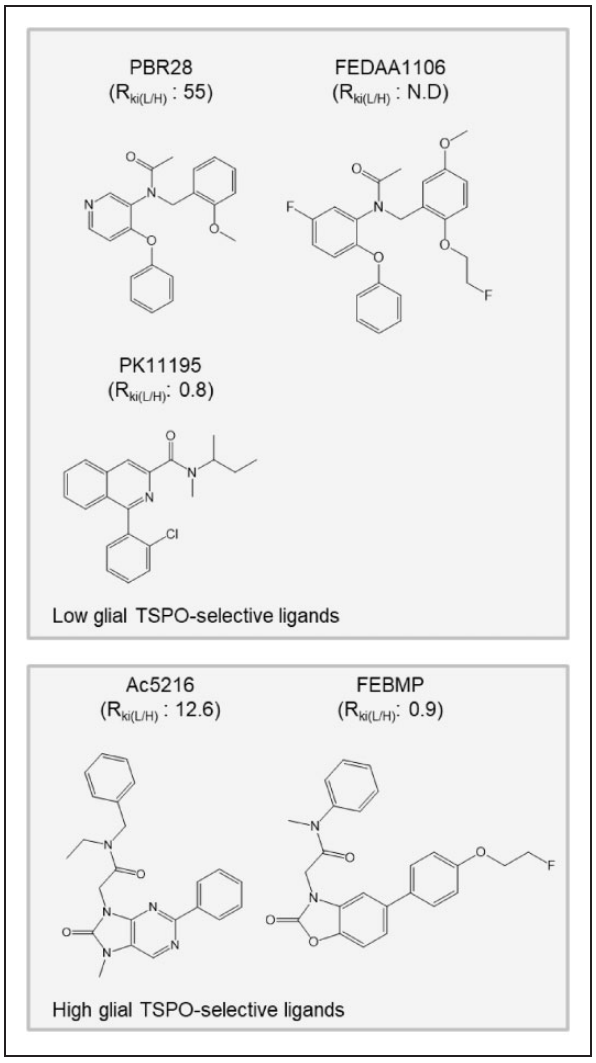

Figure 7. Classification of TSPO ligands based on preferential binding to microglia-like TSPO and influence of TSPO polymorphism (rs6971) on their binding affinity. Higher value of Ki ratio for LAB to HAB (RKi(L/H)) indicates greater influence on binding affinity of ligand. Data of RKi(L/H) are from Owen et al.[17,18] and Tiwari et al.[26]

brain regions. FEBMP and Ac5216 likely represent a class of TSPO ligand that relatively prefers to bind to glial rather than to vascular TSPO.

Collectively, this study provides the first demonstration of the differential selectivity of PET imaging agents for glial versus vascular TSPO. The higher selectivity for glial TSPO and binding sites independent of non-TSPO components likely contribute to the sensitive detection of neuroinflammation with ^{18}F-FEBMP in diseased brains, indicating the potential advantage of ^{18}F-FEBMP over other current radioligands for PET imaging of TSPO, considering its insensitivity to TSPO polymorphism based on the *in-vitro* result. Of course, given that obvious *in-vivo* sensitivity to rs6971 was observed in ^{11}C-ER176, a novel TSPO PET tracer, that had not been expected from *in-vitro* studies,[41] the *in-vitro* result of FEBMP does not necessarily mean that this will also be found *in-vivo* in humans. Further examinations based on clinical studies will be required.

Acknowledgments

The authors thank Prof. John Q. Trojanowski and Prof. Virginia M.-Y. Lee (Center for Neurodegenerative Disease Research, University of Pennsylvania) for kindly providing human tissue. We also thank Takeharu Minamihisamatsu, Sayuri Uchida, Sayuri Sasaki, Sayaka Shibata, Nobuhiro Nitta and Yoshikazu Ozawa for their assistance with the experiments at the National Institute of Radiological Sciences.

Authors' contributions

B.J., M-R. Z., I.A., T.S., M.S and M.H. designed the research; B.J., M.O., T.Y., M.F., C.S. and S.K. performed the research; N.S., M.H. and B.J. analyzed the data; B.J. and M.H. wrote the paper.

Declaration of conflicting interests

The author(s) declared no potential conflicts of interest with respect to the research, authorship, and/or publication of this article.

Funding

The author(s) disclosed receipt of the following financial support for the research, authorship, and/or publication of this article: This work was supported in part by the Strategic Research Program for Brain Sciences from the Japan Agency for Medical Research and Development, AMED, Brain/MINDS (Brain Mapping by Integrated Neurotechnologies for Disease Studies), COI (Center of Innovation) Stream for MRI devices by AMED, and JSPS KAKENHI Grand Number 15K09979.

Supplementary material

Supplemental material for this article is available online.

References

1. Cumming P, Burgher B, Patkar O, et al. Sifting through the surfeit of neuroinflammation tracers. *J Cereb Blood Flow Metab* 2018; 38: 204–224.
2. Jacobs AH, Tavitian B and Consortium IN, INMiND consortium. Noninvasive molecular imaging of neuroinflammation. *J Cereb Blood Flow Metab* 2012; 32: 1393–1415.
3. Higuchi M, Maeda J, Ji B, et al. In-vivo visualization of key molecular processes involved in Alzheimer's disease pathogenesis: Insights from neuroimaging research in humans and rodent models. *Biochim Biophys Acta* 2010; 1802: 373–388.

4. Janssen B, Vugts DJ, Funke U, et al. Imaging of neuroinflammation in Alzheimer's disease, multiple sclerosis and stroke: recent developments in positron emission tomography. *Biochim Biophys Acta* 2016; 1862: 425–441.
5. Stefaniak J. and O'Brien J. Imaging of neuroinflammation in dementia: a review. *J Neurol Neurosurg Psychiatry* 2016; 87: 21–28.
6. Kreisl WC, Fujita M, Fujimura Y, et al. Comparison of [(11)c]-(r)-pk 11195 and [(11)c]pbr28, two radioligands for translocator protein (18 KDa) in human and monkey: Implications for positron emission tomographic imaging of this inflammation biomarker. *Neuroimage* 2010; 49: 2924–2932.
7. Yokokura M, Mori N, Yagi S, et al. In vivo changes in microglial activation and amyloid deposits in brain regions with hypometabolism in Alzheimer's disease. *Eur J Nucl Med Mol Imaging* 2011; 38: 343–351.
8. Okello A, Edison P, Archer HA, et al. Microglial activation and amyloid deposition in mild cognitive impairment: a pet study. *Neurology* 2009; 72: 56–62.
9. Schuitemaker A, Kropholler MA, Boellaard R, et al. Microglial activation in Alzheimer's disease: an (r)-[(1)(1)c]pk11195 positron emission tomography study. *Neurobiol Aging* 2013; 34: 128–136.
10. Groom GN, Junck L, Foster NL, et al. Pet of peripheral benzodiazepine binding sites in the microgliosis of Alzheimer's disease. *J Nucl Med* 1995; 36: 2207–2210.
11. Zhang J. Mapping neuroinflammation in frontotemporal dementia with molecular pet imaging. *J Neuroinflammation* 2015; 12: 108.
12. Golla SS, Boellaard R, Oikonen V, et al. Quantification of [18f]dpa-714 binding in the human brain: initial studies in healthy controls and Alzheimer's disease patients. *J Cereb Blood Flow Metab* 2015; 35: 766–772.
13. Maeda J, Suhara T, Zhang MR, et al. Novel peripheral benzodiazepine receptor ligand [11c]daa1106 for pet: an imaging tool for glial cells in the brain. *Synapse* 2004; 52: 283–291.
14. Maeda J, Zhang MR, Okauchi T, et al. In vivo positron emission tomographic imaging of glial responses to amyloid-beta and tau pathologies in mouse models of Alzheimer's disease and related disorders. *J Neurosci* 2011; 31: 4720–4730.
15. Endres CJ, Pomper MG, James M, et al. Initial evaluation of 11c-dpa-713, a novel TSPO PET ligand, in humans. *J Nucl Med* 2009; 50: 1276–1282.
16. Ikoma Y, Yasuno F, Ito H, et al. Quantitative analysis for estimating binding potential of the peripheral benzodiazepine receptor with [(11)c]daa1106. *J Cereb Blood Flow Metab* 2007; 27: 173–184.
17. Owen DR, Gunn RN, Rabiner EA, et al. Mixed-affinity binding in humans with 18-kda translocator protein ligands. *J Nucl Med* 2011; 52: 24–32.
18. Owen DR, Lewis AJ, Reynolds R, et al. Variation in binding affinity of the novel anxiolytic xbd173 for the 18 kda translocator protein in human brain. *Synapse* 2011; 65: 257–259.
19. Owen DR, Yeo AJ, Gunn RN, et al. An 18-kda translocator protein (TSPO) polymorphism explains differences in binding affinity of the pet radioligand pbr28. *J Cereb Blood Flow Metab* 2012; 32: 1–5.
20. Lavisse S, Garcia-Lorenzo D, Peyronneau MA, et al. Optimized quantification of translocator protein radioligand (1)(8)f-dpa-714 uptake in the brain of genotyped healthy volunteers. *J Nucl Med* 2015; 56: 1048–1054.
21. Varrone A, Mattsson P, Forsberg A, et al. In vivo imaging of the 18-kda translocator protein (TSPO) with [18f]fedaa1106 and pet does not show increased binding in Alzheimer's disease patients. *Eur J Nucl Med Mol Imaging* 2013; 40: 921–931.
22. Kreisl WC, Lyoo CH, McGwier M, et al. In vivo radioligand binding to translocator protein correlates with severity of Alzheimer's disease. *Brain* 2013; 136: 2228–2238.
23. Cosenza-Nashat M, Zhao ML, Suh HS, et al. Expression of the translocator protein of 18 KDa by microglia, macrophages and astrocytes based on immunohistochemical localization in abnormal human brain. *Neuropathol Appl Neurobiol* 2009; 35: 306–328.
24. Rizzo G, Veronese M, Tonietto M, et al. Kinetic modeling without accounting for the vascular component impairs the quantification of [(11)c]pbr28 brain pet data. *J Cereb Blood Flow Metab* 2014; 34: 1060–1069.
25. Tomasi G, Edison P, Bertoldo A, et al. Novel reference region model reveals increased microglial and reduced vascular binding of 11c-(r)-pk11195 in patients with alzheimer's disease. *J Nucl Med* 2008; 49: 1249–1256.
26. Tiwari AK, Ji B, Yui J, et al. [18f]FEBMP: positron emission tomography imaging of tspo in a model of neuroinflammation in rats, and in vitro autoradiograms of the human brain. *Theranostics* 2015; 5: 961–969.
27. Ji B, Maeda J, Sawada M, et al. Imaging of peripheral benzodiazepine receptor expression as biomarkers of detrimental versus beneficial glial responses in mouse models of Alzheimer's and other CNS pathologies. *J Neurosci* 2008; 28: 12255–12267.
28. Ji B, Chen CJ, Bando K, et al. Distinct binding of amyloid imaging ligands to unique amyloid-beta deposited in the presubiculum of Alzheimer's disease. *J Neurochem* 2015; 135: 859–866.
29. Yoshiyama Y, Higuchi M, Zhang B, et al. Synapse loss and microglial activation precede tangles in a p301s tauopathy mouse model. *Neuron* 2007; 53: 337–351.
30. Barron AM, Ji B, Kito S, et al. Steroidogenic abnormalities in translocator protein knockout mice and significance in the aging male. *Biochem J* 2018; 475: 75–85.
31. Yasuno F, Kosaka J, Ota M, et al. Increased binding of peripheral benzodiazepine receptor in mild cognitive impairment-dementia converters measured by positron emission tomography with [(1)(1)c]daa1106. *Psychiatry Res* 2012; 203: 67–74.
32. Yasuno F, Ota M, Kosaka J, et al. Increased binding of peripheral benzodiazepine receptor in Alzheimer's disease measured by positron emission tomography with [11c]daa1106. *Biol Psychiatry* 2008; 64: 835–841.
33. Cumming P, Pedersen MD, Minuzzi L, et al. Distribution of pk11195 binding sites in porcine brain studied by autoradiography in vitro and by positron emission tomography. *Synapse* 2006; 59: 418–426.

34. Garnier M, Dimchev AB, Boujrad N, et al. In vitro reconstitution of a functional peripheral-type benzodiazepine receptor from mouse Leydig tumor cells. *Mol Pharmacol* 1994; 45: 201–211.
35. Delavoie F, Li H, Hardwick M, et al. In vivo and in vitro peripheral-type benzodiazepine receptor polymerization: functional significance in drug ligand and cholesterol binding. *Biochemistry* 2003; 42: 4506–4519.
36. Papadopoulos V, Baraldi M, Guilarte TR, et al. Translocator protein (18KDa): new nomenclature for the peripheral-type benzodiazepine receptor based on its structure and molecular function. *Trends Pharmacol Sci* 2006; 27: 402–409.
37. McEnery MW, Snowman AM, Trifiletti RR, et al. Isolation of the mitochondrial benzodiazepine receptor: association with the voltage-dependent anion channel and the adenine nucleotide carrier. *Proc Natl Acad Sci USA* 1992; 89: 3170–3174.
38. Manczak M and Reddy PH. Abnormal interaction of vdac1 with amyloid beta and phosphorylated tau causes mitochondrial dysfunction in Alzheimer's disease. *Hum Mol Genet* 2012; 21: 5131–5146.
39. Cuadrado-Tejedor M, Vilariño M, Cabodevilla F, et al. Enhanced expression of the voltage-dependent anion channel 1 (vdac1) in Alzheimer's disease transgenic mice: an insight into the pathogenic effects of amyloid-beta. *J Alzheimers Dis* 2011; 23: 195–206.
40. Ramirez CM, Gonzalez M and Diaz M. VDAC and Eralpha interaction in caveolae from human cortex is altered in Alzheimer's disease. *Mol Cell Neurosci* 2009; 42: 172–183.
41. Ikawa M, Lohith TG, Shrestha S, et al.; Biomarkers Consortium Radioligand Project Team. 11c-er176, a radioligand for 18-kda translocator protein, has adequate sensitivity to robustly image all three affinity genotypes in human brain. *J Nucl Med* 2017; 58: 320–325.